In: K.-H. Hoffmann, R.H.W. Hoppe, V. Schulz (eds.):
Fast Solution of Discretized Optimization Problems (Birkhäuser Verlag, 2001) 221-241.

Numerical Optimal Control Strategies for Semi-Active Vehicle Suspension with Electrorheological Fluid Dampers

Uwe Rettig and Oskar von Stryk

Abstract. Optimal control problems for semi-active vehicle suspensions and their numerical solution are discussed in this paper. For this purpose, several models of the vehicle dynamics with different levels of details and a general formulation of different sub-criteria for rating the ride comfort and safty are presented and investigated in this paper. The benefits and drawbacks of various numerical optimal control methods such as LQR-, H^∞ and direct collocation when applied to the different optimal control problems for semi-active vehicle suspension are investigated. Furthermore, the semi-active vehicle suspension is based on a dynamic model of the recently developed prototype of a continuously controllable shock absorber with a smart, electrorheological fluid. These are smart materials and have been known for already more than 50 years. They belong to the group of colloidal suspensions which are able to change their viscosity drastically. This depends upon molecular chain formations in the fluid caused by an electric field perpendicular to the direction of flow. Very low control costs and fast response times of the ERF devices have sparked much an interest in ERFs in the last couple of years. The development of new control strategies for ERF devices integrated into complex multi body systems require a high level of knowledge of the behavior of the ERF subsystems. Dynamic models of controllable ERF devices are studied with respect to their particular dependencies, effects and requirements. An application is presented here which merges linear optimal control strategies and ERF shock absorbers within a complex model of full car dynamics. Here we give a mathematical formulation for the objectives of ride comfort and safety that takes into account various measurement possibilities. The result demonstrates the large potential of optimally controlled ERF devices.

1. Introduction

Electrorheological fluids (ERF) change their viscosity depending on an externally applied electrical field strength. An analogous phenomenon exists for the viscosity of magnetorheological fluids which depends on the applied magnetic field strength. The bandwidth of the resulting flow properties is large; the state varies between

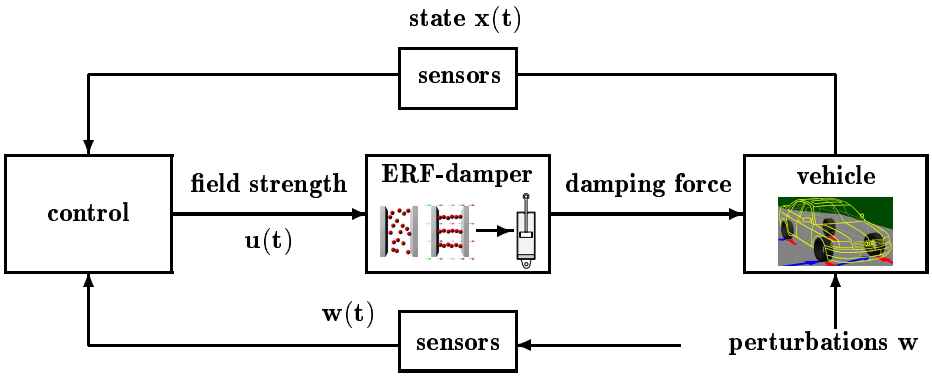

FIGURE 1. Submodels and flow chart of control, perturbation, and state variables for the problem of optimal semi-active vehicle suspension using ERF shock absorbers.

fluid and nearly solid material. The phenomenon of these fluids, caused by polarizable particles within a nonconducting carrier fluid which disturb the flow when excited, has been known since the late 1950's [2]. Hence flow, shear and squeeze processes can be controlled using easily generated electrical fields. ERF devices have additionally several advantageous control properties. The response time between one and 15 ms is extremely fast. Furthermore, ERF devices are continuously controllable and operate subject to almost no wear.

ERF devices thus represent an excellent class of interfaces between electronic control units and mechanical components which have gained increased scientific and economic interest in recent years. As a result, new generations of ERFs with optimized properties are now available. In particular, the difficulties like stability over long time periods and sedimentation of the polarizable particles have largely been resolved. The application areas for ERF devices are numerous. High frequencies and forces may be relatively easily controlled using flexible electronic units. Already many different applications have been reported [7] including a prototype of an adaptively controllable ERF-shock absorber by Schenck AG, Darmstadt.

There are two major problems which arise when investigating the simulation and optimal control of the continuously controllable ERF-shock absorbers and their application to (semi-)active vehicle damping. First there lies the question of modeling and simulating the dynamic behavior of ERF-shock absorbers which depend on the applied electrical field. Second, with regards to the computation of controls that maximize safety and comfort, suitable models for the vehicle dynamics and the safety and comfort objectives must be developed together with applicable numerical methods (Figure 1). A control framework which serves well

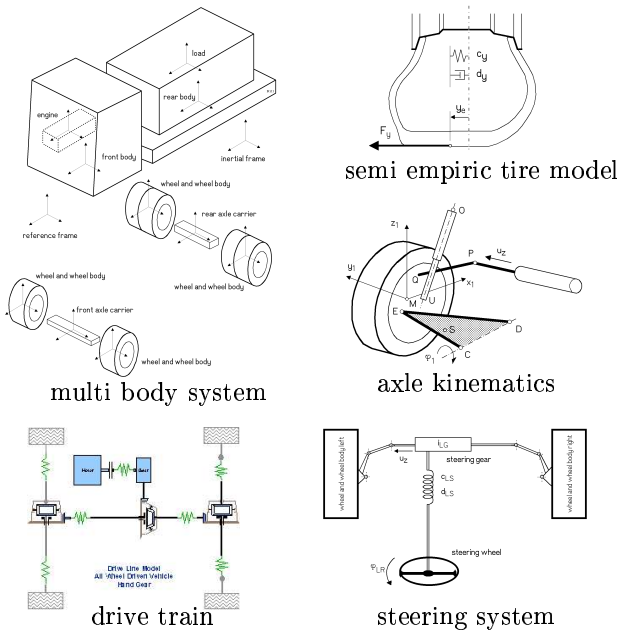

FIGURE 2. Submodels of the full motor vehicle dynamics model of VEDYNA

to evaluate the potential of semi-active damping with optimally controlled ERF-shock absorbers is that of deterministic optimal control methods which provide an open-loop optimal trajectory numerically. For its application in a semi-actively suspended vehicle, feedback controls must be computed under real-time conditions and, thus, the control will likely only be suboptimal.

2. Optimal Control Problems for Optimal Semi-Active Suspension

2.1. Models of Motor Vehicle Dynamics

Motor vehicles are very complex systems which include many significant components for its dynamical driving behavior and yield a high number of degrees of freedom. A detailed and comprehensive vehicle model is needed to represent the nonlinear kinematics of the wheel and axle and to describe the drive train, the steering mechanism, the tire dynamics and ground contact forces [12, 18]. Depending upon the specific design purpose for the dynamical model, a reduction of the system dimension can often be achieved. The influence of the neglected components of the full model are interpreted then as general perturbations of the reduced system.

2.1.1. FULL VEHICLE DYNAMICS MODEL The numerical, real-time simulation of a full motor vehicle dynamics model that accounts for all significant effects is

used in our investigations to verify optimal and suboptimal controls that have been computed using reduced and small scale models of the vehicle dynamics. Our vehicle model consists of a suitable multibody system with kinematical connections and force elements which is supplemented by a sophisticated tire model. A general purpose modeling approach to multibody systems based on the descriptor form of the equations of motion results in a large-scale system of differential-algebraic equations (DAEs) of index 3. However, we make use of an optimally tailored model description which yields a system of ordinary differential equations (ODEs) and is well suited for simulation in real-time.

The vehicle model of VEDYNA [9, 28] consists of a system of nine rigid bodies comprising the vehicle body, the axle suspensions and the wheels. Further submodels are employed to depict the characteristics of the drive train, the steering mechanism, and the tires (Figure 2). Suitable minimum coordinates and generalized velocities are used to describe the spatial state of the vehicle and its components. The equations of motion are derived from Jourdain's Principle yielding

$$
\begin{aligned}
M_{BV}(y_{BV})\,\dot{z}_{BV} &= Q_{BV}(y_{BV}, z_{BV}, y_{ST}, z_{ST}, y_{DT}, z_{DT}) && (1)\\
\dot{y}_{BV} &= K_{BV}^{-1}(y_{BV})\,z_{BV} && (2)\\
M_{DT}\,\dot{z}_{DT} &= Q_{DT}(y_{DT}, z_{DT}) && (3)\\
\dot{y}_{DT} &= V_{DT}\,z_{DT} && (4)\\
M_{ST}(y_{ST}, y_{BV})\,\dot{z}_{ST} &= Q_{ST}(y_{ST}, z_{ST}) && (5)\\
\dot{y}_{ST} &= V_{ST}\,z_{ST} && (6)\\
D\,\dot{y}_T &= F_{stat} - C\,y_T. && (7)
\end{aligned}
$$

Thus, the vehicle dynamics are fully characterized by the system of 24 first-order ODEs comprising the vehicle body and the axles, (1) and (2). Eight ODEs (7) describe the lateral and longitudinal deviations of the tires by means of spring and damper elements. The vertical deformations of the tires are covered by (1). The dynamic model of the drive train consists of 19 ODEs, (3) and (4), including four equations governing the angular wheel speeds. Five additional ODEs account for the dynamics of the steering system (5) and (6). Couplings between the separate systems occur via the generalized forces and torques Q_{BV}. Wind forces and moments result in additional forces applied to the multibody system of the vehicle [9, 28].

The tire forces have a significant impact on the dynamical behavior of a vehicle. The semi-empirical tire model that is used here describes the behavior of a real tire accurately [9, 28]. About 80 parameters which can be measured or estimated enter the model for each tire in VEDYNA. The model covers different driving situations, including effects at the driving limits such as sliding and spinning. The actual tire model is selected online depending on the respective road and weather conditions.

Due to the stiffness of the system (1)–(7) its numerical integration is carried out recursively with a semi-implicit one-step Euler scheme using a constant step size [9, 28]. In particular, the integration method makes efficient use of the special block structure of the ODEs. It turns out that a fast and stable solution is possible in real-time on modern PC hardware.

For a realistic implementation of virtual test-drives using the simulation, models for the driver and the road have been developed [9, 28].

2.1.2. Models of Quarter Cars and Linear Vehicle Dynamics The oscillating behavior of a vehicle excited by perturbations of the ground and driving maneuvers are investigated using *vertical dynamics models*, i.e. reduced models for vertical displacements of the vehicle and wheel bodies. The unknown maneuvers such as braking, acceleration and cornering under high velocities, if considered, may be regarded as perturbations.

Vertical models of vehicles may be classified into different levels of detail. There are so-called *full-car-models* (in the context of vertical models) including two axles, which reflect both vertical deflections and inclinations. Bounce, roll and pitch motions are investigated simultaneously. Separated and decoupled investigations are possible using *half-car-models* (cf. Figure 3, right). The inclination is

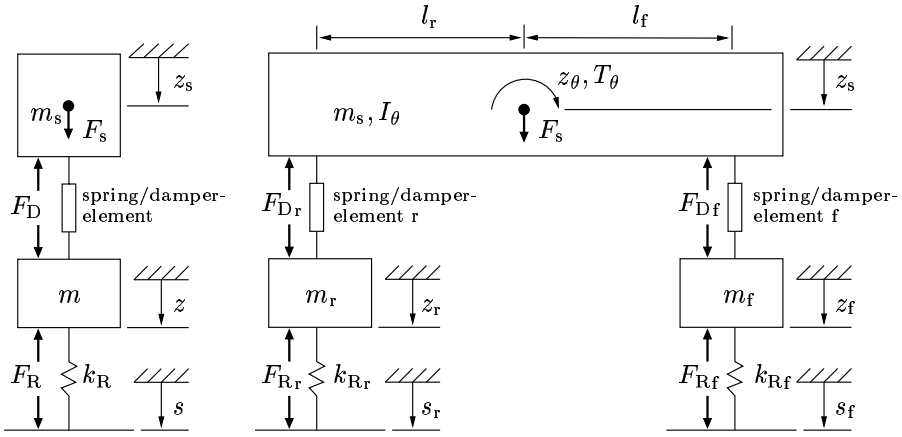

Figure 3. Quarter car model (left) and half car model (right).

variable	denotation
$z_\mathrm{s}, z_\theta, z_{r/f}$	displacement and inclination of vehicle body, displacement of the wheel
m_s, I_θ	mass and moment of inertia of the vehicle body
F_D	force at the spring/damper element
F_R	wheel load (wheel model assumed to be a spring, often in addition with a parallel damping element or as a more complex model)
$s_{\mathrm{r/f}}$	perturbation of the ground, (r - rear, f - front)
F_s, T_θ	perturbing force and moment (induced by maneuvers)

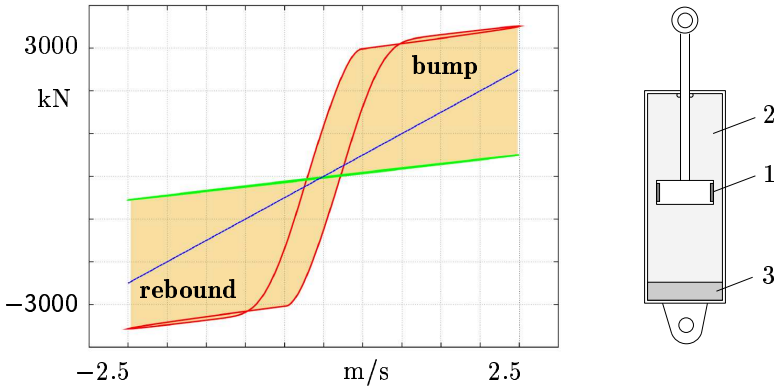

FIGURE 4. Typical ERF damper characteristics (left) under minimum and maximum excitation of the ERF, the enclosed area describes the bandwidth of adjustable damping rates compared to conventional linear damping. Sketch of a ERF damper (right), 1 - valve between the electrodes, 2 - chambers filled with ERF, 3 - gas filled accumulator. Different designs with longer electrodes are commonly used.

interpreted as roll *or* pitch motion. The most common and simple model is the *quarter-car-model* (cf. Figure 3, left), which represents the vertical motion of a system including a quarter of the vehicle body and one of the wheels. Its corresponding simplified equations will be the base of our calculations with respect to our goal of optimal semi-active suspension.

2.1.3. NONLINEAR SINGLE TRACK VEHICLE MODEL The vehicle dynamics model should also take into account the particular properties of the ERF shock absorbers. Substitution of the commonly used linear damping behavior within the models of Section 2.1.2 by a realistic dynamic model of the ERF damping characteristics yields a highly nonlinear system of differential equations (cf. Section 2.2). This may be extended by further substitutions such as nonlinear models for tires. Such a more realistic upgrade of a half car model is commonly used for calculation of different optimal controls [28]. Specially calculated damping controls take into account pitch motions which are significant for time shifted perturbations on front and rear wheels.

2.2. Dynamic Model of a Continuously Controllable ERF Shock Absorber

Conventional damping behavior is usually described by a fixed damping characteristic defined by the force-velocity rate. In general, dampers exhibit nonlinear behavior. Depending on the actual damper design, the damping rates are different in the bump and rebound phases while within each phase the system is best

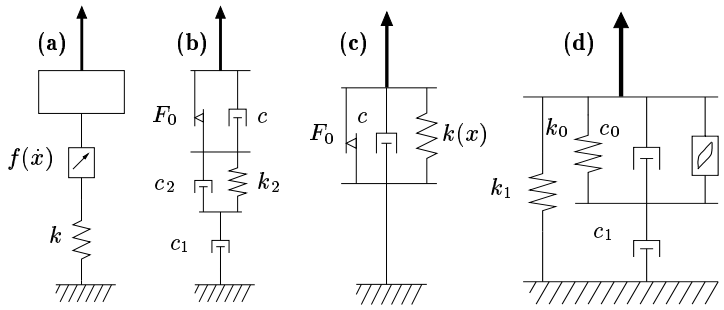

FIGURE 5. Proposed phenomenological models for ERF devices. (a) Peel, Stanway, Bullough [24] (b) Powell [19]; (c) Ehrgott, Masri [11] resp. Kamath Wereley [14]; (d) Spencer et.al. [23].

described by progressive damping characteristics. For a more realistic simulation, piecewise linear or higher order polynomial approximations of realistic tabular data are used.

Measurements of ERF dampers indicate strong nonlinear behavior and characteristics with hysteresis. The dynamics of the characteristics depend upon the damping velocity *and* on the exciting electrical field.

Poiseuille flow within the valve has already been calculated under highly simplifying assumptions (steady state, laminar, incompressible flow neglecting mass inertia, cf. [1, 20]). The results demonstrate that the *Bingham* property of the ERF, defining the ratio between shear stress and strain rate, dominates the force-velocity characteristics of the damper. A comparison of the calculated and measured damping rates also suggests the necessity for more complex simulations, including the effects of dynamic flow, particular geometry, vortices, etc.

Another approach which avoids these complex and expensive calculations are parametric models. A sufficiently precise prediction of the dynamic behavior of an ERF shock absorber using parametric models depends upon an optimal set of parameters that minimize a particular distance between model prediction and provided measurements. Of course, the type of dynamic model dominates the error between prediction and reality. General approximation techniques, for instance Čebyšev polynomials (cf. [11]) and multilayer neural networks (cf. [6, 15]) have previously been investigated. More common models are phenomenological models. Here the approximation of the ERF effects is usually induced by friction elements or nonlinear spring or damper elements (cf. Figure 5). However, only a few of them take into account the dependency on a variable electrical field. An overview is given in [7, 25].

The *augmented Bouc-Wen* model (cf. [23], see also [7, 13]), Figure 5(d)) is the most flexible one and is used in the following sections. It describes a dynamic

system depending on $\dot{z}_\mathrm{D}$, the velocity of the piston rod.

$$\begin{aligned} \dot{s}_1 &= \frac{1}{c_0 + c_1}\left(c_1 \dot{z}_\mathrm{D} - \alpha s_2 - k_0 s_1\right) \\ \dot{s}_2 &= \left(A - \beta(1 + \operatorname{sgn}(\dot{s}_1 s_2)) s_2^2\right) \dot{s}_1 \end{aligned} \tag{8}$$

The output function

$$F = c_1(\dot{z}_\mathrm{D} - \dot{s}_1) + k_1(z_\mathrm{D} - z_0) \tag{9}$$

denotes the damping force and depends on $\dot{z}_\mathrm{D}$ and z_D, the relative displacement of the damper. The system (8) describes a hysteresis operator, and its properties are parameterized with respect to the applied electrical field. This gives

$$\dot{s}_3 = \eta(u_\mathrm{D} - s_3) \tag{10}$$

with control u_D as the applied field strength and

$$\begin{aligned} c_0 &= c_{01} + s_3 c_{02} \\ c_1 &= c_{11} + s_3 c_{12} \\ \alpha &= \alpha_1 + s_3 \alpha_2 \,. \end{aligned} \tag{11}$$

The states $\mathbf{s} = (s_1, s_2, s_3)^\mathrm{T}$ denote the inner variables of the virtual model of each ERF damper. For a more realistic ERF damper model, the 11-dimensional parameter vector $\mathbf{p} = (c_{11}, c_{01}, \alpha_1, A, \beta, c_{11}, c_{02}, \alpha_2, k_0, k_1, z_0, \eta)^\mathrm{T}$ must be estimated numerically from measurements of a prototype damper.

2.3. Objectives for Comfort and Safety

2.3.1. Parameterized Cost Functional The two primary objectives for a vehicle ride with semi-active suspension are ride safety and ride comfort. For both, mathematical models must be provided.

The characterization of safety in the vehicle dynamics depends primarily on wheel loads. High loads have greater longitudinal and lateral transmission forces between wheels and ground. On the contrary, low wheel loads can cause the loss of controllability of the vehicle. Larger magnitudes for the roll and pitch angles will indirectly influence ride safety as the wheels' contact force magnitudes might reach zero causing lift-off.

The comfort of a ride can be of almost equal importance to passengers than safety. Comfort is mainly characterized by the accelerations of the vehicle body, often called the *sprung mass* contrary to the wheel body, which in this sense is called the *unsprung mass*. With respect to the vertical models (cf. Section 2.1.2), vertical accelerations are treated here. For models with a higher level of detail, angle accelerations of pitch and roll motions may also be considered.

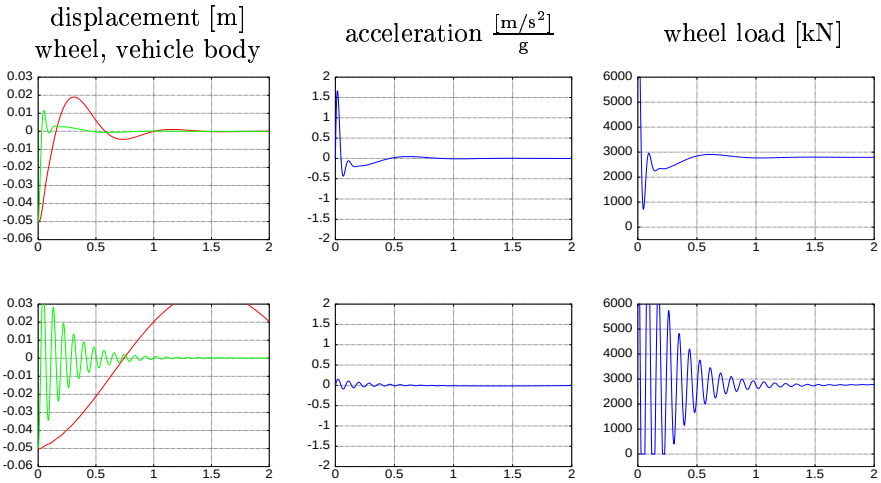

FIGURE 6. Comparison of optimal controls and trajectories resulting from the two extremes of cost functional weights. The curves in the upper row are obtained for the optimal control with respect to safety only, the lower ones for optimal control with respect to comfort only. All curves are depicted over time in [s] and are based on a quarter car model and an initial step disturbance. (wheel displacement: bright, vehicle body displacement: darc line)

Altogether a performance index consisting of a weighted sum of various criteria of safety and comfort may be used

$$L(\mathbf{x},\mathbf{u}) = \mu_{\text{safety}} \left[\sum_{i=\text{f},r} \left[\frac{F_{\text{dyn.load},i}}{F_{\text{stat.load},i}} \right]^2 + \left[\frac{z_\theta}{z_{\theta,\max}} \right]^2 \right] + \mu_{\text{comfort}} \left[\left[\frac{\ddot{z}_s}{\ddot{z}_{s,\max}} \right]^2 + \left[\frac{\ddot{z}_\theta}{\ddot{z}_{\theta,\max}} \right]^2 \right] . \tag{12}$$

For an example of the state and control variables $\mathbf{x}$ and $\mathbf{u}$, we refer to the half-car-model of Figure 3. For a full-car-model (in the sense of vertical models) one can extend the functional by terms of the second angular magnitude. The variables $F_{\text{dyn.load},i}, \ddot{z}_\text{s}, z_\theta, \ddot{z}_\theta$ denote the deviation from the corresponding stationary value.

2.3.2. THE WEIGHTS The weights $\mu_\diamond$ have to be chosen properly, i.e. depending on the purpose of investigation. For example, their actual value may depend on the actual driving situation where either comfort or safety may be more desirable. Figure 6 shows suspension behavior under different optimal semi-active damping with respect to either only safety or comfort. Here, the purpose is to demonstrate the antagonistic character of the two goals. Optimized safety leads to fast regulation of the oscillations under high accelerations of the vehicle body, whereas optimized

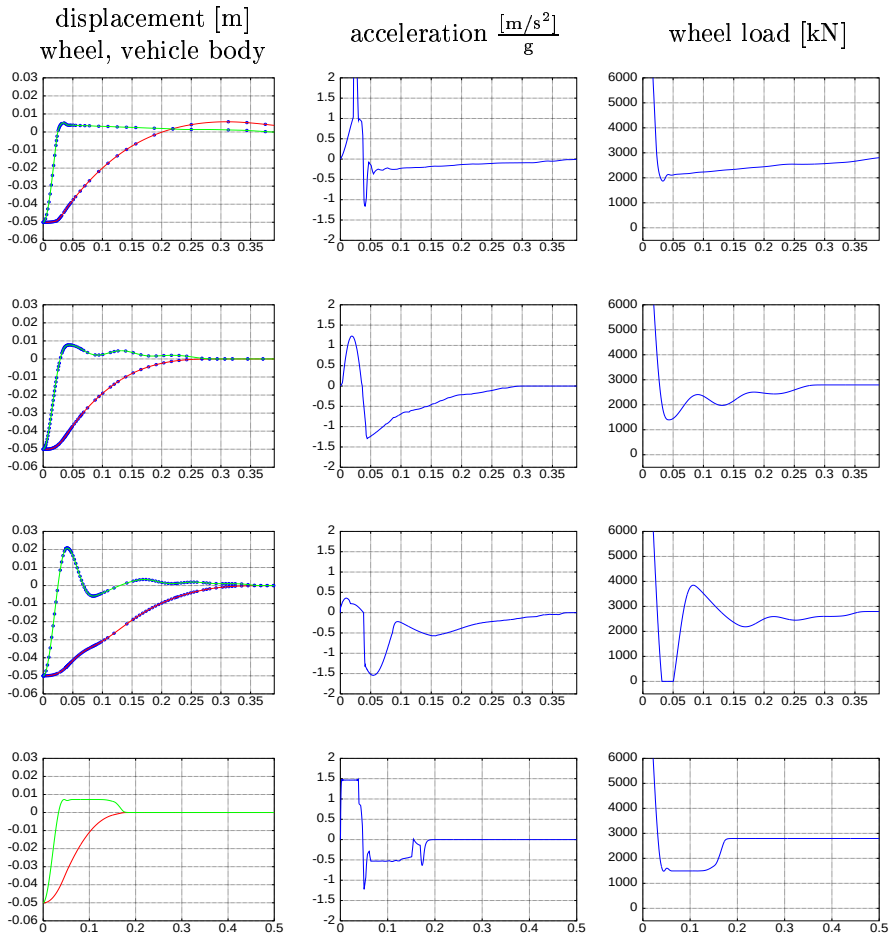

FIGURE 7. Comparison of curves by different optimization configurations (all curves over time in [s], wheel displacement: bright line, vehicle body displacement: darc line).
first row: optimal safety, comfort ignored
second row: optimal comfort with constrained wheel load
third row: optimal comfort, safety ignored
fourth row: version with a slack variable.

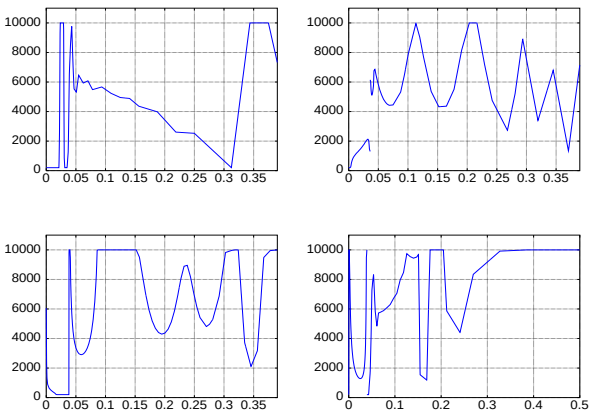

FIGURE 8. Controls corresponding to the four rows depicted in Figure 7 (damping rates over time in [s]: upper row, left - one; upper row, right - two; lower row, left - three; lower row, right - four).

comfort yields almost decoupled motions of vehicle and wheel body under very low accelerations of the sprung mass and high frequencies of the unsprung mass. Please note the periods of time intervals of contact losses to the ground.

2.3.3. DIFFERENT VERSIONS OF OBJECTIVES Evidently it is not possible to simultaneously ensure a maximum value for the respective cost functionals corresponding to both safety and comfort by choosing particular weights of the cost functional

$$L = \mu_{\text{safety}} L_{\text{safety}} \quad + \quad \mu_{\text{comfort}} L_{\text{comfort}}.$$

Another approach to handle this problem is to optimize one of the objectives and to restrict the other one to suitable bounds.

$$\min L_1 \qquad \text{under} \qquad L_2 \leq L_{2,\max}.$$

This approach usually yields satisfactory results. A third approach is to maximize a positive slack variable σ which is subtracted from both objective values of safety and comfort

$$\max \sigma \qquad \text{under} \qquad L_i \leq L_{i,\max} - \sigma, \quad i = 1, 2 \quad \sigma > 0\,.$$

Each difference is then constrained to a proper maximum value. Figure 7 shows the behavior of the state variables of a quarter car model for the resulting optimal controlled semi-active suspension. Although the displacement state variable shows similar behavior for the first three examples, the optimal damping rates are very different (see Figure 8). The last optimization configuration using a slack variable yields high gain damping.

Optimization with respect to safety		
constant parameters	18.85	
semi-active damping	11.57	(61,4%)
active damping	7.05	(37,4%)

Values derived by general nonlinear calculation of optimal damping forces for a quarter car model with respect to occurring inequality constraints.

TABLE 1. Comparison of optimal values of the cost functionals for different damping configurations.

However, weighting remains a subjective task. Sporty racing cars, ambulance vehicles or ordinary automobiles have to be designed by different requirements.

3. Numerically Calculated Controls and Results

The goal of the control problem for controllable ERF-shock absorbers integrated into a semi-active vehicle suspension is a combination of optimal safety and optimal comfort of the ride. Nowadays available standard techniques for damping control are rather simple: The driver or a control unit selects a fixed damping characteristic from several optional settings. The new technology of ERF-shock absorbers permits continuous control. This supposes the calculation of suitable (if possible optimal) controls taking into account the dynamics of the vehicle and of the damper (Section 2.1). The resulting dynamical system may be highly nonlinear and further constraints have to be taken into account.

3.1. State Feedback Controller based on LQR and H^∞ Techniques

In order to test the capability of semi-active damping with ERF-shock absorbers, state feedback controls for various linearized, reduced vehicle models (cf. Section 2.1.2) were computed and implemented. The general problem formulation for a linear vehicle dynamics model is written as

$$\dot{\mathbf{x}} = \underbrace{\begin{pmatrix} \mathbf{0}_{n_x,n_x} & \mathbf{I}_{n_x,n_x} \\ \mathbf{M}^{-1}\mathbf{A}_\mathrm{k} & \mathbf{M}^{-1}\mathbf{A}_\mathrm{c} \end{pmatrix}}_{\mathbf{A}} \mathbf{x} + \underbrace{\begin{pmatrix} \mathbf{0}_{n_x,n_u} \\ \mathbf{M}^{-1}\mathbf{B}_\mathrm{m} \end{pmatrix}}_{\mathbf{B}} \mathbf{u} + \underbrace{\begin{pmatrix} \mathbf{0}_{n_x,n_g} \\ \mathbf{M}^{-1}\mathbf{D}_\mathrm{m} \end{pmatrix}}_{\mathbf{D}} \mathbf{g}, \tag{13}$$

with zero matrix $\mathbf{0}$, unit matrix $\mathbf{I}$, mass matrix $\mathbf{M}$, stiffness matrix $\mathbf{A}_\mathrm{k}$, damping matrix $\mathbf{A}_\mathrm{c}$, control matrix $\mathbf{B}_\mathrm{m}$ and perturbation matrix $\mathbf{D}_\mathrm{m}$. The state $\mathbf{x}$ is controlled by $\mathbf{u}$ and perturbed by $\mathbf{g}$, $n_\diamond$ denote their dimensions, $\diamond = x, u$, or g. Perturbations include shocks caused by an uneven ground as well as forces and moments acting on the vehicle body caused by driving maneuvers. The linear quadratic cost functional

$$J[\mathbf{u}] = \int_0^\infty \mathbf{x}^\mathrm{T}\mathbf{Q}\,\mathbf{x} + 2\mathbf{u}^\mathrm{T}\mathbf{S}\,\mathbf{x} + \mathbf{u}^\mathrm{T}\mathbf{R}\,\mathbf{u}\;\mathrm{d}t \tag{14}$$

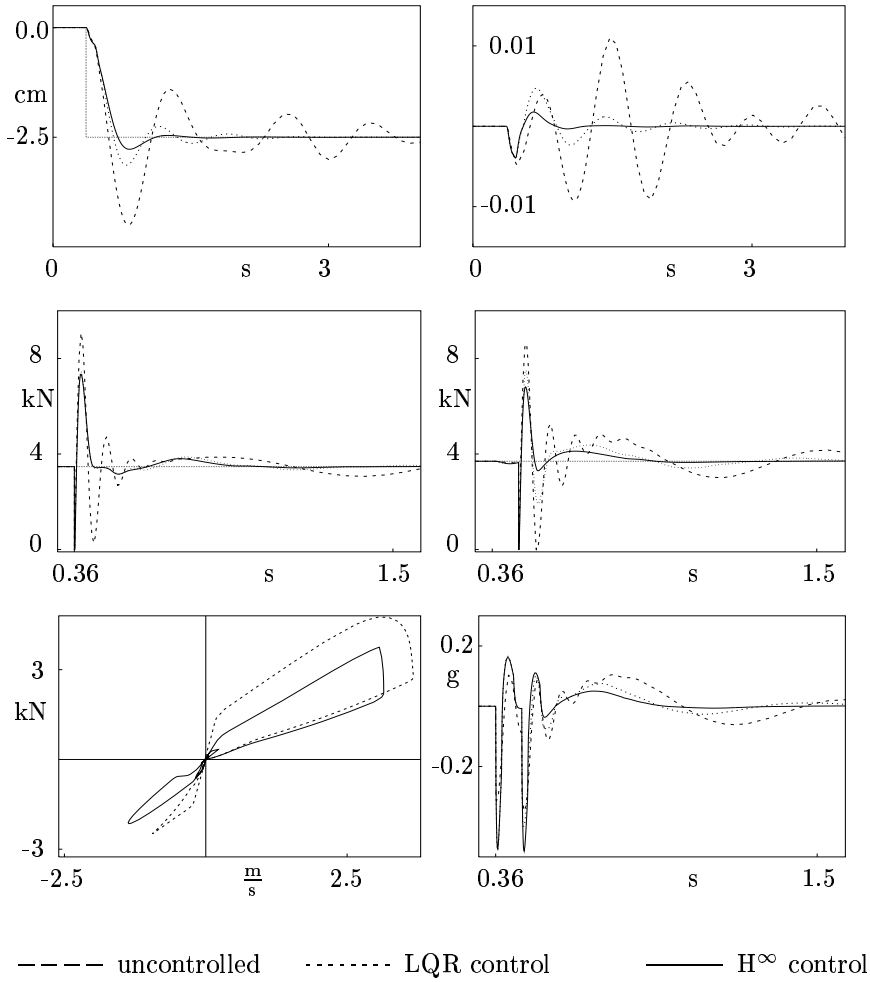

FIGURE 9. Comparison of some of the state variables of a single track model for a ride over a step of 2.5 cm height at a speed of 100 km/h for different controls.

upper left	motion of center of gravity of the sprung mass	z_s
upper right	curve of the pitch angle	z_θ
middle left	wheel load of the front wheel	$F_{\mathrm{R}f}$
middle right	wheel load of the rear wheel	$F_{\mathrm{R}r}$
lower left	front(-·-) and rear (–) characteristics	$F_{\mathrm{D}r/f}$
lower right	sprung mass accelerations	$\ddot{z}_s$

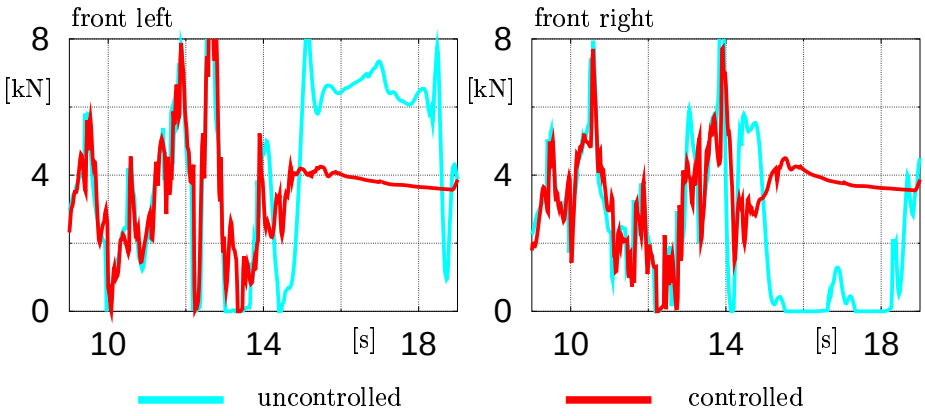

FIGURE 10. Wheel loads on right and left front wheels of the full vehicle dynamics model for a controlled and uncontrolled ride within the critical phase.

again is a weighted criterion for safety and comfort with

$$\begin{aligned}
\mathbf{Q} &= \mu_{\text{comfort}} \sum_{\substack{\text{vehicle body}\\ \text{velocities}}} \frac{1}{\ddot{z}^2_{i,\max}} \mathbf{A}^{\mathrm{T}} \mathbf{e}_i \mathbf{e}_i^{\mathrm{T}} \mathbf{A} + \mu_{\text{safety}} \sum_{\text{wheels}} \left[\frac{k_{\mathrm{R}i}}{F_{\text{stat.load},i}} \right]^2 (\mathbf{e}_i \mathbf{e}_i^{\mathrm{T}}) \\
&\quad \ldots + \sum_{\text{states}} \mu_{i,\text{state}} \frac{1}{x^2_{i,\max}} (\mathbf{e}_i \mathbf{e}_i{}^{\mathrm{T}}) \\
\mathbf{R} &= \mu_{\text{comfort}} \sum_{\substack{\text{vehicle body}\\ \text{velocities}}} \frac{1}{\ddot{z}^2_{i,\max}} \mathbf{B}^{\mathrm{T}} \mathbf{e}_i \mathbf{e}_i^{\mathrm{T}} \mathbf{B} + \mu_{\text{costs}} \sum_{\text{wheels}} \frac{1}{u_{i,\max}} \mathbf{B}^{\mathrm{T}} \mathbf{e}_i \mathbf{e}_i^{\mathrm{T}} \mathbf{B} \\
\mathbf{S} &= \mu_{\text{comfort}} \sum_{\substack{\text{vehicle body}\\ \text{velocities}}} \frac{1}{\ddot{z}^2_{i,\max}} \mathbf{B}^{\mathrm{T}} \mathbf{e}_i \mathbf{e}_i^{\mathrm{T}} \mathbf{A}.
\end{aligned}$$

The optimal active damping force can now be obtained by

$$\mathbf{u}^* = -\mathbf{K}\mathbf{x} = \mathbf{R}^{-1}(\mathbf{S} + \mathbf{B}^{\mathrm{T}}\mathbf{P})\mathbf{x} \tag{15}$$

with the solution $\mathbf{P}$ of the algebraic Riccati equation corresponding to the cost functional of Equation (14). Expanding the approach of conventional optimal control (LQR, cf. [5, 10, 16]), H^∞ control techniques include the worst influence of occurring perturbations (cf. [3, 10, 13]). Here the extreme (optimal resp. pessimistic) controls are saddle-point solutions of the dynamic game with the parameterized cost functional

$$J_\gamma[\mathbf{u}, \mathbf{g}] = \int_0^\infty \mathbf{x}^{\mathrm{T}}\mathbf{Q}\,\mathbf{x} + 2\mathbf{u}^{\mathrm{T}}\mathbf{S}\,\mathbf{x} + \mathbf{u}^{\mathrm{T}}\mathbf{R}\,\mathbf{u} - \gamma^2\mathbf{g}^{\mathrm{T}}\mathbf{g}\;\mathrm{d}t\,, \tag{16}$$

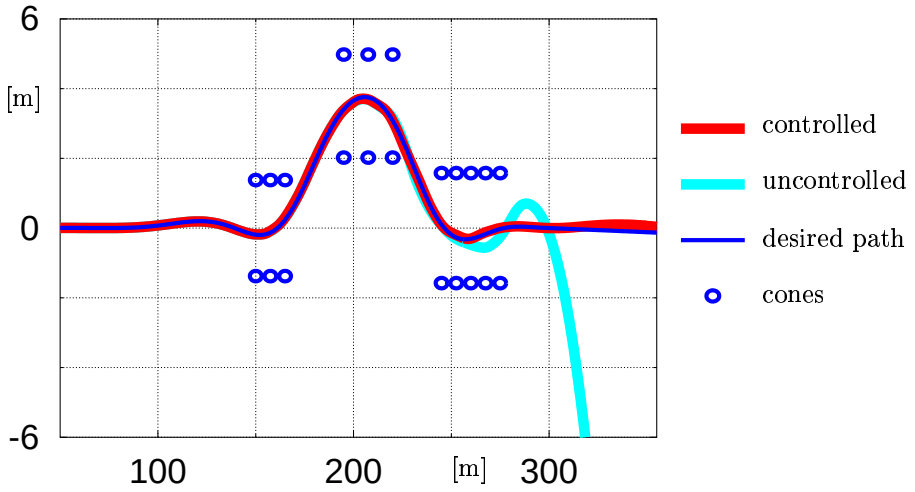

FIGURE 11. Double lane change maneuver (path through the cones) on a very uneven street simulated with the full vehicle dynamics model. The uncontrolled car, i.e. with a conventional passive suspension, swerves off the road whereas the controlled car, i.e. with an (sub-)optimally controlled semi-active suspension, follows the desired time optimal path.

where $\mathbf{u}$ is the minimizing and $\mathbf{g}$ is the maximizing player. For $\gamma > 0$ and optimal $\mathbf{u}^0 = \mathbf{u}^0(\mathbf{g})$ we have $J\left[\mathbf{u}^0; \mathbf{g}\right] / \|\mathbf{g}\|^2 \leq \gamma^2 \quad \forall \mathbf{g}$, i.e. the disturbance of the system is bounded. The optimal disturbance attenuation is related to a minimal bound γ^*, which is calculated iteratively. Since the existence of an optimal controller for the "infimum" is not guaranteed, suboptimal solutions for $\gamma = \gamma^* + \varepsilon$ may be sought for (see [13]). Both the approaches LQR and H^∞ are feasible and yield useful damping performances (cf. Figure 10).

3.2. Verification within a Dynamic Full Car Simulation

The linearity of the problem formulation merely allows the calculation of the optimal damping force but not the optimal damping rate or field strength at the valve of the ERF-shock absorber as in the general nonlinear case. Hence the application of ordinary algorithms for *linear quadratic regulators* causes active damping. Technically speaking this requires energy input into the vehicle suspension system which is not supported by the technique of ERF-shock absorbers. Table 1 shows the difference between optimal cost functionals under various damping configurations. Please note that obtaining the best performance with fully active damping must in practice be payed with a substantially more expensive technical effort than for semi-active damping.

Based on the calculated optimal damping force (Section 3.1), a prediction of a capable semi-active damping rate is computed by a heuristic compensation regulator. A "clipped optimal" algorithm is suggested in [22]. Here a related approach

$$u = \begin{cases} u_{\min} \text{ for } F_{\text{opt}} F_{\text{appl}} < 0 \\ \min(u_{\max}, \max(u_{\min}, u + (|F_{\text{opt}}| - |F_{\text{appl}}|) * K)) \text{ otherwise} \end{cases} \tag{17}$$

is applied with the requested optimal active force F_{opt} and the current force F_{appl} for each ERF damper. It is assumed that an estimate of F_{appl} is available. The constant K depends on the scaling of u.

Generally in this context, the measurability and observability of the state variables is important. In addition to an estimate of F_{appl}, the damping velocities of the shock absorber and the vehicle body accelerations are assumed to be given, e.g., by measurements. A *Kalman state estimator* is used to provide state estimates for the system (13), cf. [10].

The calculated feedback controllers are verified within the real-time full car simulation VEDYNA (Section 2.1.1), which includes 56 dynamic state variables in its basic version and accounts for the most relevant effects of a complex vehicle model. A typical test maneuver for vehicles, the *double lane change*, cf. Figure 11, simulated on a very uneven street demonstrates the improvement in safety. A car equipped with an ERF-shock absorber remains on a commanded minimum time path through the cones (cf. [28]), whereas the conventional car begins to slide. Higher wheel loads are provided by controlled vehicle suspensions as shown in Figure 10.

3.3. Nonlinear deterministic optimization

3.3.1. The Direct Collocation Method as implemented in Dircol, cf. [26], computes the numerical solution for general, nonlinear optimal control problems with the following general problem formulation

$$\min J[u] = \Phi(x(t_{\text{f}}), t_{\text{f}})$$

$$\begin{array}{rrcl} & \dot{x}(t) & = & f(x(t), u(t), t) \\ \text{under} & 0 & = & r(x(0), x(t_{\text{f}}), t_{\text{f}}) \\ & 0 & \leq & g(x(t), u(t), t), \quad 0 \leq t \leq t_{\text{f}}. \end{array} \tag{18}$$

The method belongs to the class of direct transcription methods [4]. The optimal control $u^*(t)$ and trajectory $x^*(t)$ minimize the cost functional J subject to the given inequality and boundary constraints and subject to the differential equations. Tasks with cost functionals of different types, namely with an integral part, have to be transformed into a problem with a Mayer-type objective, cf. Equation (18). The discretization process approximates the controls $u(t)$ on a time grid $\{t_k : t_0 \leq t_k < t_{k+1} \leq t_n = t_{\text{f}}\}$ by a continuous, piecewise linear function; the states $x(t)$ are interpolated by continuously differentiable cubic functions on the same time grid. Dircol further permits the modeling of multiple phases used for switching dynamics or controls. In this case, the time interval is decomposed within each

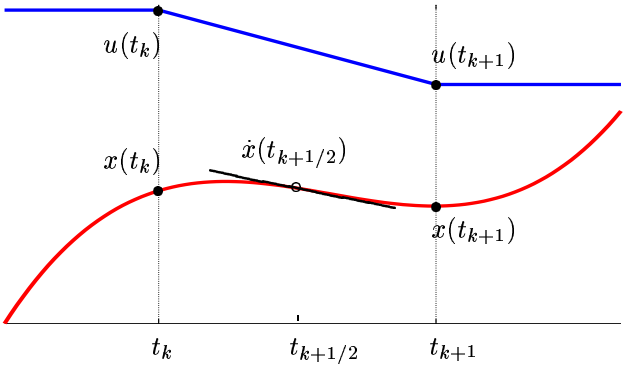

FIGURE 12. Principle of the direct collocation method

phase. This yields additional conditions on the phase transitions. In order to save expensive writing effort a one phase problem is described here. The discretization scheme leads to

$$\begin{aligned} &\min\ J[u] = \Phi(x(t_\mathrm{f}), t_\mathrm{f}) \\ &\begin{array}{lcll} f(t, x(t), u(t)) & = & \dot{x}(t) & \forall t = t_{k+1/2} \\ r(x(t_0), x(t_\mathrm{f})) & = & 0 & \\ g(t, x(t), u(t)) & \geq & 0 & \forall t = t_k. \end{array} \end{aligned} \tag{19}$$

For $Y = \big(x(\tau_0), u(\tau_0), \ldots, x(\tau_n), u(\tau_n), t_\mathrm{f}\big)$ a *nonlinearly constrained minimization problem* results in

$$\begin{aligned} &\min \Phi(Y) \\ &a(Y) = 0 \\ &b(Y) \geq 0\,. \end{aligned} \tag{20}$$

Solutions of (20) are currently obtained by *SQP-methods*. If structure and sparsity of the NLP functions and their gradients are exploited and the large-scale SQP method SNOPT [21] is applied, a computational speed-up and storage savings by two orders of magnitude can be obtained [27].

3.3.2. RESULTS Several local error estimators are investigated to monitor the accuracy of the computed approximation of the solution and the need for a local grid refinement. The estimates of the adjoint variables $\tilde{\lambda}$ and the multipliers $\tilde{\mu}$ of the constraints resulting from the optimal control problem and calculated from the Lagrangian multipliers of the discretized minimization problem make the following

calculation possible

$$\tilde{\omega}_k = \int_{t_k}^{t_{k+1}} \tilde{\lambda}(t)\Big(f(\tilde{x}(t),\tilde{u}(t),t) - \dot{\tilde{x}}(t)\Big) + \tilde{\eta}(t)g(\tilde{x}(t),\tilde{u}(t),t)\mathrm{d}t \qquad (21)$$

for $k = 1,\ldots,n-1$. The sum of the values $\tilde{\omega}_k$, called the *optimality error*, vanishes for exact optimal solutions $\tilde{x} = x^*$, $\tilde{u} = u^*$ and exact multipliers $\tilde{\lambda} = \lambda^*$, $\tilde{\mu} = \mu^*$. Furthermore, *defects* of the differential equations and of the nonlinear constraints

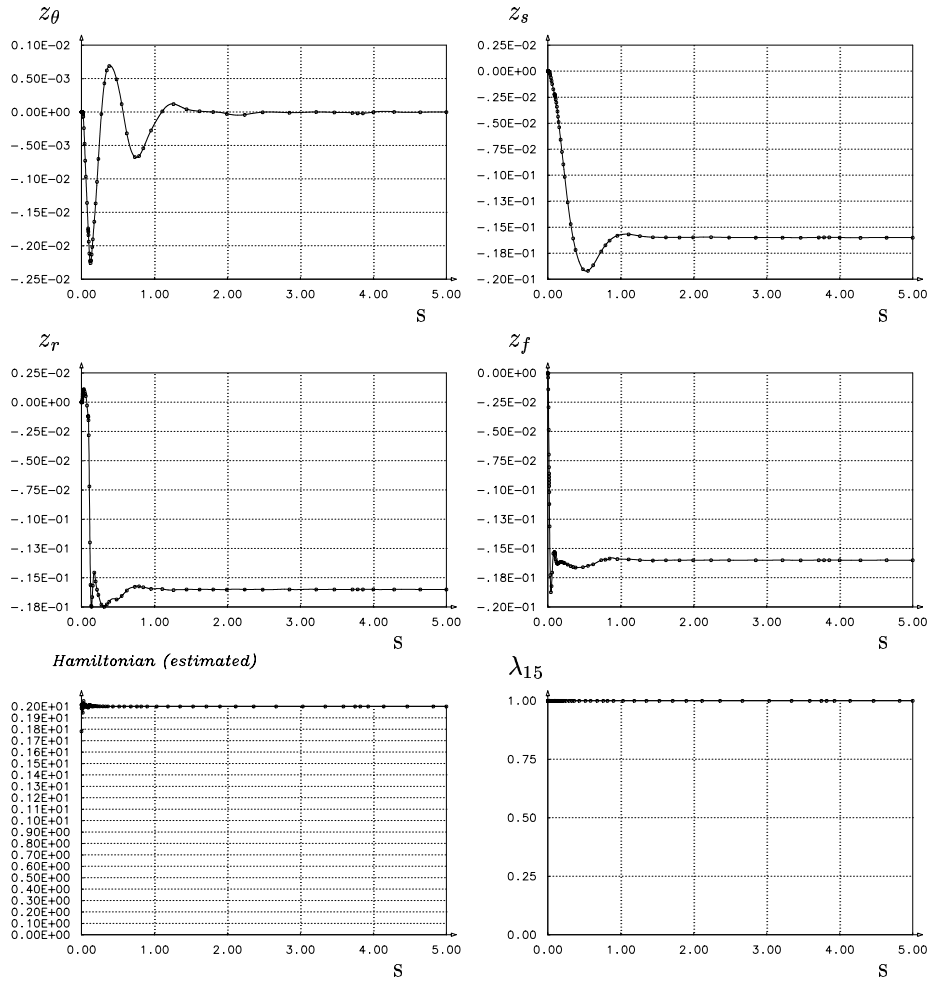

FIGURE 13. Calculated results of an optimal semi-active damping control for a single track vehicle model equipped with ERF shock absorber during a ride over a step (speed 100 km/h). The solutions shows the 68 marked grid points.

are evaluated at the points $t = t_{k+l/4}$, $l = 0, 1, 2, 3$ (cf. [26, 27]). These error estimators are used for an automatic iterative grid refinement which can produce more exact and robust solutions. This yields problems with a high number of grid points; nevertheless, they can be calculated very fast with the sparse version of DIRCOL.

Figure 13 depicts a calculated example. Here the lower figures show the estimated Hamiltonian and the adjoint variable for the scaled time variable. These trajectories demonstrate the high accuracy of the solutions although adjoint differential equations have neither been formulated nor solved numerically. The location of the marked grid points are obtained by evaluation of the error estimators in the sequence of solutions.

4. Conclusions

The problem of optimal semi-active suspension of vehicles using the new technology of electrorheological fluid dampers has been investigated. For the formulation of the corresponding optimal control problems, several models of the vehicle dynamics with different levels of detail for the ERF shock absorber dynamics and the safety and comfort objectives are presented and investigated.

Reduced, linear vehicle dynamic models permit the application of LQR and H^∞ control techniques which provide an optimal and real-time capable feedback control for the reduced model. The resulting controls are only suboptimal with respect to the full scale vehicle dynamics model but provide remarkable improvements over passive suspensions as has been demonstrated in numerical experiments. In spite of the improvements (in particular for the ride safety), significant nonlinearities in the dynamics of the ERF-suspensions continue to counteract the calculated control, whereby the potential of the ERF technology can not fully be exploited by this approach. On the other hand, direct transcription methods can deal with general, nonlinear dynamic models and constraints, but they only provide optimal open-loop state and control trajectories.

Furthermore, it has been demonstrated that comfort and safety have antagonistic properties. Several ways to deal with comfort and safety in a single objective have been investigated and discussed here.

Future work will focus on nonlinear H^∞ control and the approximation of optimal feedback controls in the case of general nonlinear dynamics.

References

[1] R.J. Atkin, Xiao Shi, W.A. Bullough: *Solutions of the constitutive equations for the flow of an electrorheological fluid in radial configurations*, Journal of Rheology, **35**(7) (1991), pp. 1441-1461.

[2] H.T. Banks, R.C. Smith, Y. Wang: *Smart Material Structures — Modeling, Estimation and Control*, (J. Wiley & Sons, 1996).

[3] T. Basar, P. Bernhard: *H^∞-Optimal Control and Related Minimax Design Problems Problems, A Dynamic Game Approach*, (Berlin: Birkhäuser, 1991).

[4] J.T. Betts: *Survey of numerical methods for trajectory optimization*, AIAA J. Guidance, Control, and Dynamics **21**, 2 (1998) 193-207.

[5] A.E. Bryson, Y.C. Ho: *Applied Optimal Control*, (Ginn and Company, 1969; Rev. printing, Hemisphere, 1975).

[6] S.A. Burton, N. Makris, I. Konstantopoulos, P.J. Antsaklis: *Modeling the response of ER damper: phenomenology and emulation*, Journal of Engineering Mechanics, **122** (1996), pp. 897-906.

[7] T. Butz, O. von Stryk: *Modelling and simulation of electro- and magnetorheological fluid dampers.* Z. Angew. Math. Mech. (2001, to appear).

[8] J.D. Carlson, B.F. Spencer Jr.: *Magneto-rheological fluid dampers: scalability and design issues for application to dynamic hazard mitigation*, in Proc. Intern. Workshop on Structural Control, Hong Kong, Dec. 18-20, 1996 to appear.

[9] C. Chucholowski, M. Vögel, O. von Stryk, T.-M. Wolter: *Real time simulation and online control for virtual test drives of cars.* In: H.-J. Bungartz, F. Durst, Chr. Zenger (Hrsg.): High Performance Scientific and Engineering Computing. Lecture Notes in Computational Science and Engineering **8** (Springer-Verlag, 1999) 157-166.

[10] P. Dorato, C. Abdallah, V. Cerone: *Linear-Quadratic Control — An Introduction*, (Englewood Cliffs, N.J.: Prentice-Hall, 1995).

[11] R.C. Ehrgott, S.F. Masri: *Modelling the oscillatory dynamic behavior of electrorheological materials in shear.* Smart Material Structures **1** (1992) 275-285.

[12] G. Genta: *Motor Vehicle Dynamics, Modelling and Simulation*, Series on Advances in Mathematics for Applied Sciences **43** (London: World Scientific, 1997).

[13] R.H.W. Hoppe, G. Mazurkevitch, U. Rettig, O. von Stryk: *Modeling, simulation, and control of electrorheological fluid devices.* In: H.-J. Bungartz et al. (eds.): Lectures on Applied Mathematics (Springer-Verlag, 2000) 251-276.

[14] G.M. Kamath, N.M. Wereley: *A nonlinear viscoelastic-plastic model for electrorheological fluids.* Smart Material Structures **6** (1997) 351-359.

[15] B. Kim, P.N. Roschke: *Linearization of Magnetorheological Behavior Using a Neural Network*, Proc. of the American Control Conf., San Diego, June 1999, pp. 4501-4505.

[16] W. Kortüm, P. Lugner: *Systemdynamik und Regelung von Fahrzeugen* (Springer, 1994).

[17] B. Koslik, G. Rill, O. von Stryk, D.E. Zampieri: *Active suspension design for a tractor by optimal control methods.* Preprint SFB-438-9801, Sonderforschungsbereich 438, Technische Universität München – Universität Augsburg (1998)

[18] M. Mitschke: *Dynamik der Kraftfahrzeuge*, (Springer Verlag, 1994).

[19] J.A. Powell: *Modelling the oscillatory response of an electrorheological fluid*, Smart Material Structures **3** (1994) 416-438.

[20] K.R. Rajapogal, A.S. Wineman: *Flow of electrorheological materials*, Acta Mechanica, **91** (1992), pp. 57-75.

[21] P.E. Gill, W. Murray, M.A. Saunders: *User's Guide for SNOPT 5.3: A Fortran Package for Large-Scale Nonlinear Programming.* Draft, Department of Mathematics, University of California, San Diego (December 1998). Software Version 5.3-5 (June 1999).

[22] B.F. Spencer Jr., S.J. Dyke, M.K. Sain, J.D. Carlson: *Modeling and control of magnetorheological dampers for seismic response reduction*, Smart Materials and Structures, **5** (1996) 565-575.

[23] B.F. Spencer Jr., S.J. Dyke, M.K. Sain, J.D. Carlson: *Phenomenological model of a magnetorheological damper*, ASCE Journal of Eng. Mech., **123**(3) (1996) 1-9.

[24] R. Stanway, D.J. Peel, W.A. Bullough: *Dynamic modelling of an ER vibration damper for vehicle suspension applications*, Smart Material Structures **5** (1996) 591-606.

[25] R. Stanway, J. L. Spronston, A. K. El-Wahed: *Applications of electrorheological fluids in vibration control: a survey*, Smart Material Structures **5** (1995) 464-482.

[26] O. von Stryk: *User's Guide for DIRCOL Version 2.1: a direct collocation method for the numerical solution of optimal control problems.* Lehrstuhl M2 Höhere Mathematik und Numerische Mathematik, Technische Universität München (1999)

[27] O. von Stryk: *Numerical Hybrid Optimal Control and Related Topics.* Habilitationsschrift, Technische Universität München (2000).

[28] M. Vögel, O. von Stryk, R. Bulirsch, T.-M. Wolter, C. Chucholowski: *An optimal control approach to real-time vehicle guidance.* submitted for publication.

Zentrum Mathematik,
Technische Universität München,
80290 München, Germany
E-mail address: `rettig@ma.tum.de`

Fachgebiet Praktische Simulation und Systemoptimierung
Technische Universität Darmstadt,
Alexanderstr. 10,
64283 Darmstadt, Germany
E-mail address: `stryk@informatik.tu-darmstadt.de`